



Finite strain visco-elastic growth driven by nutrient diffusion: theory, FEM implementation and an application to the biofilm growth

Meisam Soleimani¹

Received: 15 March 2019 / Accepted: 17 April 2019 / Published online: 27 April 2019
© Springer-Verlag GmbH Germany, part of Springer Nature 2019

Abstract

In this paper, a thermodynamically consistent visco-elastic growth model driven by nutrient diffusion is presented in the finite deformation framework. Growth phenomena usually occur in biological tissues. Systems involving growth are known to be open systems with a continuous injection of mass into the system which results in volume expansion. Here the growth is driven by the diffusion of a nutrient. It implies that the diffusion equation for the nutrient concentration needs to be solved in conjunction with the conservation equation of mass and momentum. Hence, the problem falls into the multi-physics class. Additionally, a viscous rheological model is introduced to account for stress relaxation. Although the emergence of residual stresses is inherent to the growth process, the viscous behaviour of the material determines to what extent such stresses remain in the body. The numerical implementation is performed using the symbolic tool Ace-Gen while employing a fully implicit and monolithic scheme.

Keywords Visco-elasticity · Biological growth · Finite strain · Biofilm growth

1 Introduction

Unlike structural material, biological tissues are able to change their geometry and internal structure even when they are not subjected to mechanical loads. Such processes are referred to as either growth or “remodeling”. Healing in a cracked bone and development of tumors are examples of biological tissue remodeling and growth, respectively. Soft tissues like tumors, biofilms and arteries generally experience growth, while hard tissues such as bone and teeth undergo remodeling. However in some cases, such as arteries, both processes might take place simultaneously. Roughly speaking, in a growth process the mass generation leads to an increase in the volume, whereas in remodeling the volume remains almost constant and the micro structure of the tissue changes, instead. For the remodeling case, the material behavior is characterized by a constitutive approach, see [7,15]. In case of growth a kinematic approach in conjunction with a constitutive model is utilized, see [8,16]. Biological tissues undergoing growth and remodeling involve strong

coupling of different physical phenomena. Several distinct types of physics such as mass transport, nutrient diffusion and mechanical deformation are governed by the associated equations in a coupled fashion. Here the focus is on the volumetric growth driven by nutrient diffusion using a combined constitutive-kinematic approach.

The key idea for modeling the mechanics of volumetric growth has been borrowed from the central idea of finite strain plasticity by decomposing the deformation gradient into an inelastic growth and an elastic part. In an analogy with elastoplastic deformations, a strain energy function is defined based on the elastic part and the growth part is governed by an evolution equation translating the mass resorption at a material point. The local nature of the growth-elastic decomposition inherently creates residual stresses in the body so as to accommodate to the incompatible growth-related deformation. This is the cost for maintaining the continuity of the solid, see [35]. In the presence of dissipative processes such as viscous effects in large time scales, residual stresses may diminish.

Tailoring available FEM-based tools or numerical codes for deformable solids to those undergoing growth requires careful attention. The reason is that the growth phenomena have to be characterized in the context of an open system in which mass can cross the boundary of the reference volume. In other words, the mass conservation equation needs

✉ Meisam Soleimani
soleimani@ikm.uni-hannover.de

¹ Institute of Continuum Mechanics, Leibniz Universität Hannover, Hannover, Germany

to be solved, unlike an ordinary deformable solid in which this equation is trivial and consequently it is not explicitly resolved. Such a mass source complicates the momentum equation, since any mass source is also an inherent momentum source. Furthermore, it is even reflected in the outcome of the angular momentum equation and determines whether the well-known Cauchy stress remains symmetric or not. Additionally, any assumed constitutive equation should be thermodynamically consistent in the sense that the second law of thermodynamics is not violated. Interested readers may refer to [11] for more details on theoretical framework of growth.

The diffusion induced growth is a matter of investigation among researchers in different areas. In [38] the folding patterns of brain as a growing soft tissue have been studied while a diffusion-reaction equation has been employed to model the cell migration and proliferation. Similar wrinkled morphology has been observed in the growth of bacterial macroscopic colonies (biofilms) in [37]. Under scarcity of the nutrient, biofilms may exhibit more complex shapes referred to as “finger patterns” [18]. In [39] the growth of tumor has been investigated using a fourth order equation of Cahn-Hilliard-type coupled with reaction-diffusion equations for the substrate components. More sophisticated growth model driven by the diffusion are presented in [5] and [1] that are based on characterizing the fluid transport through a chemical potential. Such models are used to capture the swell or squeeze of elastomeric hydro-gels embedded in a solvent. Under critical conditions, instabilities in the geometry of the swollen hydro-gels bring even more complication in such a diffusion-driven growth process [10]. Since the objective of developing our diffusion-driven growth model is to employ it in biofilm simulations, the numerical examples are entirely related to this area. Nonetheless, one can use the developed model with minor modifications in other applications such as tumor growth or hydrogel swelling. The significance of biofilms in medical and industrial application is undeniable. They might be either harmful or advantageous. The formation of dental plaque on the teeth surface that may result in an infection in the oral cavity [28] is an example of detrimental biofilms. On the contrary, the beneficial biofilms are the main actors in water treatment system [13] in which the toxic substances are removed from the waste water. Interested readers may refer to [23] for an up-to-date review of the current application of biofilms.

As mentioned before, biofilm growth is also an example of the growth process driven by the nutrient diffusion. It is a complex process in the sense that several physical phenomena are coupled and consequently different time-scales are involved. An argument about the order of magnitude related to the different time scales in biofilm processes can be found in [27]. This leads to the assumption that all fast processes (smaller time scales) such as nutrient diffusion

reach their steady state values when a slower process (large time scale) such as biofilm growth is taking place. Early attempts to mathematically model biofilms can be traced back to 1980s, see [30] in which a one dimensional system of partial differential equation describes the biofilm growth. Since then, a various number of methods has been proposed to model two and three dimensional biofilms, all of which fall into either continuum-based [3,9,26] or hybrid discrete-continuous models that are known as Individual-Based Methods (IBM) [20,21,25]. In the second group, the overall behavior and spatial structure of biofilms is a result of biological interactions at the individual level between discrete agents. The presented method is entirely continuum-based and in the framework of the Finite Element Method (FEM).

The author has already developed a numerical tool for modeling biofilms, especially biofilm growth, based on the Smoothed Particle Hydrodynamics (SPH) method, see [34]. In the previous work, biofilms were treated in a hypo-elastic approach and a staggered explicit solution scheme was employed, whereas in the present paper a finite visco-hyperelastic formulation is chosen along with a fully monolithic and implicit procedure. The objective of this work is to develop further the theory of finite-elastic growth presented in [16] to be employed in biofilm simulation. There are two main novelties in this regard. Firstly, the theory is extended and reviewed in order to accommodate the viscous effects using the framework introduced in [17]. Secondly, an additional scalar field variable is introduced for the diffusion of a nutrient as the driver of the growth. A fully implicit and monolithic scheme is employed to solve the resulting multi-physics problem.

2 On the theory of visco-elastic growth mechanics

2.1 Kinematics of growth

To start with the mathematical framework, we consider the well known deformation map in continuum mechanics as a body, see Fig. 1. Let \mathcal{B}_0 be the initial configuration of the body. \mathbf{F} is the local deformation gradient that relates an infinitesimal material line element from \mathcal{B}_0 to its map in the deformed configuration \mathcal{B}_t at time t . In fact the motion of the body during the time interval $[0, T]$ is given by $\mathbf{x} = \varphi(\mathbf{X}, t)$ and \mathbf{F} is essentially the tangent of this map defined as $\mathbf{F} = \frac{\partial \mathbf{x}}{\partial \mathbf{X}}$. In this formulation, the deformation from \mathcal{B}_0 to \mathcal{B}_t is decomposed into two steps. First the material points are mapped into a newly grown, stress-free state. It means that an intermediate auxiliary configuration \mathcal{B}_g is introduced. The collection of these grown states is denoted \mathcal{B}_g and is not necessarily compatible i.e., parts of the body may intersect. The

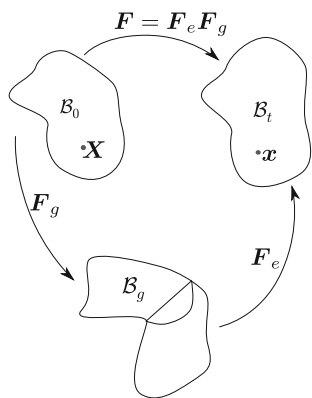


Fig. 1 Multiplicative decomposition of deformation gradient in finite growth

second step applies an elastic deformation to the incompatible state B_g , obtaining the state B_t which may now contain residual stresses in order to accommodate the incompatibility of the previous state and maintain the continuity of the solid body. Such model yields a multiplicative split of the gradient deformation tensor

$$F = F_e F_g. \tag{1}$$

This decomposition is formally analogous to the well-known decomposition of elasto-plastic deformation gradient into its elastic and plastic parts and was first introduced in biomechanics by [31]. While the mass generation is assumed to take place only between the states B_0 and B_g , the elastic response occurs only between B_g and B_t . In fact the state B_g is assumed to be stress free. Now, one needs to construct the F_g . Volume change during growth can be specified by

$$J_g = \det(F_g) = \frac{V_g}{V_0}, \tag{2}$$

with V_g and V_0 being the local tissue volumes before and after the growth increment, respectively. It is common to assume that the new tissue constituents are deposited in all directions equally (isotropic growth) and hence F_g has the form

$$F_g = J_g^{\frac{1}{3}} I = \alpha I, \tag{3}$$

in which I is the identity tensor and $\alpha := J_g^{\frac{1}{3}}$.

Now we have to relate the stimuli of growth to the growth tensor by means of a phenomenological description. Several variables can be regarded as growth stimulus such as stress, concentration field of a chemical agent and so on. Exactly here is the point of departure from the constitutive equation presented in [16]. In the present work, the growth is assumed to be driven solely by the concentration of a chemical agent denoted by a scalar field variable C . The constitutive equation

is governed by the so-called Monod law [30] which relates the rate of generated mass (volume) to the concentration according to

$$\dot{\alpha} = Y \frac{K_1 C}{K_2 + C}, \tag{4}$$

where Y , K_1 and K_2 are biological constants and C is the concentration of the nutrient. This constitutive equation is widely used in the biofilm growth. Equation (4) actually reflects bacteria growth due to nutrient (food) consumption. C is governed by the diffusion equation.

In practice, Eq. (4) is discretized in time so that the value of α can be found. Here a backward Euler method is employed according to

$$\frac{\alpha_{n+1} - \alpha_n}{\Delta t} = Y \frac{K_1 C_{n+1}}{K_2 + C_{n+1}}. \tag{5}$$

When it comes to the concentration field C , in analogy with the heat transport equation, the associated weak form for C in the spatial coordinate (in B) reads

$$\int_B D \text{grad}(C) \cdot \text{grad}(\delta C) dv + \int_{\partial B} q^C \cdot n \delta C ds = 0, \tag{6}$$

where grad refers to the gradient operator in the spatial configuration and D is the diffusivity tensor which is commonly assumed to be spatially isotropic. It means that it is defined as $D = DI$ with I being the second order identity tensor. Moreover, δC is a virtual variation of the concentration field C . Additionally, q^C stands for the spatial concentration flux and n is the normal of the boundary. It should be noted that the time dependent part is absent in Eq. (6) due to the time scale argument which was discussed in the introduction. One can express the weak form with respect to the material coordinate (in B_0) by invoking the Piola transformation $\text{grad}(\bullet) = F^{-T} \text{Grad}(\bullet)$ as follows

$$\int_{B_0} D \text{Grad}(C) \cdot \text{Grad}(\delta C) J dV + \int_{\partial B_0^C} Q^C \cdot N \delta C dS = 0, \tag{7}$$

in which N is the normal to the boundary in the initial configuration which is related to n through the well-known Nanson’s formula. Similarly, Q^C is the material counterpart of q^C .

The weak form of mechanical balance equation (linear momentum conservation) governs the other unknown field variable u . In practice, u plays the role of the primal variable which characterizes the deformation φ through $\text{Grad} \varphi = F = I + \text{Grad} u$ with I being the identity tensor. It can be written in the initial configuration as

$$\int_{\mathcal{B}_0} \frac{1}{2} \mathbf{S} : \text{Grad} \delta \mathbf{C} dV + \int_{\partial \mathcal{B}_0^u} \mathbf{PN} \cdot \delta \mathbf{u} dS = 0, \tag{8}$$

in which \mathbf{P}, \mathbf{S} correspond to first and second Piola-Kirchhoff stress, respectively. Furthermore, \mathbf{C} denotes right Cauchy strain tensor. It is obvious that the expression \mathbf{PN} accounts for the traction boundary condition. We need to emphasize that here the use of usual balance of linear momentum (without extra terms due to the growth) is permissible due to the assumption of “slow growth”, see [14]. Otherwise, the extra terms associated with the momentum source are not negligible and should be taken into account in Eq. 8.

REMARK: It is worthwhile to recognize that the coupling between mechanical deformation \mathbf{u} and concentration field C happens via two mechanisms: firstly, the growth part of the deformation gradient tensor is a function of the concentration field [see Eqs. (3) and (4)] and secondly, the postulation of fulfilling the diffusion equation in the current configuration [see Eq. (6)] will lead to another interlocking between the mechanical deformation and concentration via the Piola transformation upon transforming the weak form into the initial coordinate [see Eq. (7)]. It entails a consistent linearization in the Newton-Raphson procedure and this is taken care of by using AceGen and its automatic differentiation capability.

At this point, one needs to assume a free energy function from which the stress can be extracted. Since the mass of a control volume changes due to the growth, the free energy density is expressed with respect to unit mass ($\hat{\Psi}$) rather than commonly used unit volume (Ψ). One can write

$$\hat{\Psi} = \hat{\Psi}(\hat{\mathbf{C}}, \hat{\mathbf{F}}, \hat{\rho}) = \frac{1}{\hat{\rho}} \Psi(\hat{\mathbf{C}}, \hat{\mathbf{F}}), \tag{9}$$

where $\hat{\mathbf{C}} = \mathbf{F}_e^T \mathbf{F}_e$ is the right Cauchy-Green tensor constructed by the elastic part of the deformation. Furthermore, a hat over it signifies that the variable lies in the intermediate configuration. Additionally, $\hat{\mathbf{F}}$ is an internal variable for the viscous effects and can be perceived as a strain-like tensor analogous to strain tensor $\hat{\mathbf{C}}$. It should be noted that $\hat{\rho}$ is the density in the intermediate configuration including added mass due to growth. This variable accounts for the growth contribution in the free energy. It is related to the density in the reference configuration via

$$\rho_0 = J_g \hat{\rho} = \alpha^3 \hat{\rho}. \tag{10}$$

Combining Eqs. (10) and (9), energy density per unit reference volume (Ψ_0) can be computed using

$$\Psi_0 = \rho_0 \hat{\Psi} = J_g \Psi. \tag{11}$$

The remaining point is to model the rate dependent viscous effects which here are reflected in $\hat{\mathbf{F}}$. Generally, there are two

possibilities to deal with the viscoelasticity: either to use a linear evolution equation for the so-called non-equilibrium part of the stress or a nonlinear one. The former is termed “finite linear viscoelasticity”, see [33] and [17]. The latter is referred as the “finite viscoelasticity”, see [32] and [29]. The second approach entails extending the multiplicative decomposition of the gradient deformation to account for the viscous-related part and consequently introducing an additional intermediate configuration. That is why we adopt the first approach in which a rheological model composed of linear spring and dash-pots, is extended to finite elasticity. To characterize the viscoelastic behaviour, the free energy function is postulated as follows

$$\Psi = \Psi(\hat{\mathbf{C}}, \hat{\mathbf{F}}) = \Psi^\infty(\hat{\mathbf{C}}) + \gamma(\hat{\mathbf{C}}, \hat{\mathbf{F}}). \tag{12}$$

In the limit where $t \rightarrow \infty$, viscous effects fade away and the free energy of an elastic body is recovered. The superscript \bullet^∞ denotes function which characterizes a purely hyper-elastic response being governed by the following equation

$$\Psi^\infty(\hat{\mathbf{C}}) = \frac{\lambda}{2} (J_e - 1)^2 + \frac{\mu}{2} \left((\text{tr}(\hat{\mathbf{C}}) - 3) + 2 \log(J_e) \right), \tag{13}$$

where λ and μ denote the elastic Lamé-constants and $J_e = \det(\mathbf{F}_e)$. It should be noted that unlike $\Psi^\infty(\hat{\mathbf{C}})$ an explicit form for the $\gamma(\hat{\mathbf{C}}, \hat{\mathbf{F}})$ is neither needed nor it is possible to compute this function. In practice, its derivative with respect to the strain measure plays a role in the stress computation procedure and dissipation equation. Such a derivative is treated as an internal variable which evolves according to an evolution equation.

With the assumption of an isothermal process, one can examine the thermodynamical consistency of the model. The dissipation of the process per unit reference volume according to the second law of thermodynamics is given by

$$\mathcal{D}_{int} = \mathbf{S} : \dot{\hat{\mathbf{C}}} / 2 - \dot{\Psi}_0 + \theta \mathcal{S}_0 \geq 0. \tag{14}$$

Here, Ψ_0 is the free energy density per unit reference volume introduced in Eq. (11). The expression $\theta \mathcal{S}_0$ is a non-negative additional term in the dissipation equation comparing to the well-known form of this equation. It accounts for the entropy production due to the openness of the system. It means that, the system exchanges mass with its environment in addition to the energy. In this expression θ and \mathcal{S}_0 stand for the absolute temperature and extra entropy source per unit volume, receptively. This source of entropy is referred to as a “non-compliant” source in [14]. It will be later shown that the presence of this extra term is necessary in case of growth driven by nutrient diffusion.

Using Eq. (11), one can rewrite Eq. (14) as follows

$$\mathcal{D}_{int} = \mathbf{S} : \dot{\mathbf{C}}/2 - J_g \dot{\Psi} - \dot{J}_g \Psi + \theta \mathcal{S}_0. \tag{15}$$

By means of the push forward operator

$$\hat{\mathbf{C}} = \mathbf{F}_g^{-T} \mathbf{C} \mathbf{F}_g^{-1}, \tag{16}$$

and the time derivative (denoted by $\hat{\square}$) identity

$$\dot{\Psi} = \partial_{\hat{\mathbf{C}}} \Psi : \hat{\dot{\mathbf{C}}} + \partial_{\hat{\mathbf{F}}} \Psi : \hat{\dot{\mathbf{F}}}, \tag{17}$$

one can expand Eq. (15) as

$$\begin{aligned} \mathcal{D}_{int} = & \left(\mathbf{S} - 2J_g \mathbf{F}_g^{-1} \frac{\partial \Psi}{\partial \hat{\mathbf{C}}} \mathbf{F}_g^{-T} \right) : \dot{\mathbf{C}}/2 \\ & + \left(2J_g \hat{\mathbf{C}} \frac{\partial \Psi}{\partial \hat{\mathbf{C}}} \mathbf{F}_g^{-T} \right) : \dot{\mathbf{F}}_g \\ & - \dot{J}_g \Psi - J_g \partial_{\hat{\mathbf{F}}} \Psi : \hat{\dot{\mathbf{F}}} + \theta \mathcal{S}_0 \geq 0. \end{aligned} \tag{18}$$

Invoking the standard argument known as ‘‘Coleman and Noll method’’ [6], one can say that since Eq. (18) must hold for all admissible processes, a constitutive equation for the second Piola Kirchhoff stress can be obtained according to

$$\mathbf{S} = 2J_g \mathbf{F}_g^{-1} \frac{\partial \Psi}{\partial \hat{\mathbf{C}}} \mathbf{F}_g^{-T}. \tag{19}$$

where one can imagine that the fictive stress $\hat{\mathbf{S}} = 2J_g \frac{\partial \Psi}{\partial \hat{\mathbf{C}}}$ has been transformed from the intermediate configuration to the initial configuration using a pull-back operator. Following the procedure introduced in [17] and in an analogy with the linear spring-dashpot system, in the evaluation of Eqs. (18) and (19) one takes $2J_g \partial_{\hat{\mathbf{C}}} \gamma = -J_g \partial_{\hat{\mathbf{F}}} \gamma = \hat{\mathbf{Q}}$ where $\hat{\mathbf{Q}}$ is a stress-like measure which characterizes the viscous response and is a work conjugate of $\hat{\mathbf{F}}$. Furthermore, using the identity

$$\left(2J_g \hat{\mathbf{C}} \frac{\partial \Psi}{\partial \hat{\mathbf{C}}} \mathbf{F}_g^{-T} \right) : \dot{\mathbf{F}}_g = \left(2J_g \hat{\mathbf{C}} \frac{\partial \Psi}{\partial \hat{\mathbf{C}}} \right) : \dot{\mathbf{F}}_g \mathbf{F}_g^{-1}, \tag{20}$$

one can rewrite Eq. (18) as follows

$$\mathcal{D}_{int} = \hat{\mathbf{M}} : \hat{\mathbf{L}}_g - J_g \text{tr}(\hat{\mathbf{L}}_g) \Psi + \hat{\mathbf{Q}} : \hat{\dot{\mathbf{F}}} + \theta \mathcal{S}_0 \geq 0, \tag{21}$$

in which $\hat{\mathbf{M}} = \hat{\mathbf{C}} \hat{\mathbf{S}}$ is called Mandel stress in the intermediate configuration whose work conjugate is the growth velocity gradient $\hat{\mathbf{L}}_g = \dot{\mathbf{F}}_g \mathbf{F}_g^{-1}$ in the intermediate configuration. It is obvious that \dot{J}_g in Eq. (18) has been replaced with $J_g \text{tr}(\hat{\mathbf{L}}_g)$ in Eq. (21). To understand the physical interpretation of this term, one can write the mass conservation equation in the reference configuration as

$$\frac{D}{Dt} \int_{\mathcal{B}_0} \rho_0 dV = \int_{\mathcal{B}_0} \mathcal{R}_0 dV, \tag{22}$$

where \mathcal{R}_0 reflects the mass production (mass source) rate per unit reference volume due to the growth.

The local form of Eq. (22) can be written as

$$\frac{D\rho_0}{Dt} = \mathcal{R}_0. \tag{23}$$

Recalling the constant density assumption in growth process ($\dot{\rho}_0 = 0$) and differentiating (10) with respect to time yields

$$\frac{D\rho_0}{Dt} = \hat{\rho}_0 J_g \text{tr}(\hat{\mathbf{L}}_g) = \rho_0 \text{tr}(\hat{\mathbf{L}}_g). \tag{24}$$

Comparing Eqs. (23) and (24) one can note that the mass source \mathcal{R}_0 is related to $\hat{\mathbf{L}}_g$ via

$$\mathcal{R}_0 = \rho_0 \text{tr}(\hat{\mathbf{L}}_g). \tag{25}$$

It means that defining the evolution equation for the growth part is equivalent to the definition of the mass source term and this way they are consistent.

One can rewrite Eq. (21) using the identity $\text{tr}(\hat{\mathbf{L}}_g) = \hat{\mathbf{L}}_g : \mathbf{I}$ (with \mathbf{I} being the second order identity tensor) in a more compact form as

$$\mathcal{D}_{int} = -\hat{\Sigma} : \hat{\mathbf{L}}_g + \mathbf{Q} : \hat{\dot{\mathbf{F}}} + \theta \mathcal{S}_0 \geq 0. \tag{26}$$

in which $\hat{\Sigma} := J_g \Psi \mathbf{I} - \hat{\mathbf{M}}$ is called Eshelby stress as the driving stress measure of the growth here. It is commonly utilized in biological growth [11] and also non-volume preserving plasticity [4]. Comparing to metal plasticity in which the volume is preserved during the plastic deformation ($J_g = 1$ or equivalently $\dot{J}_g = 0$), one realizes that in metal plasticity Mandel stress appears in dissipative term pertaining to the plastic deformation rather than Eshelby stress. If one follows the sequence of Eqs. (14) to (26) with careful scrutiny, it can be understood that the emergence of Eshelby stress in growth is an immediate result of $\dot{J}_g \neq 0$. Unlike metal plasticity, growth is not an isochoric process and that is why the proper dissipative work conjugate of the growth velocity gradient $\hat{\mathbf{L}}_g$ is Eshelby stress $\hat{\Sigma}$ not Mandel stress $\hat{\mathbf{M}}$ which some authors come up with, see for example [16]. A similar discussion has been presented in [4] about the non-volume preserving plasticity which is similar to the growth phenomena.

Following the argument presented in [16], one can find a thermodynamically consistent choice for the entropy source term \mathcal{S}_0 in Eq. (26) by taking

$$-\hat{\Sigma} : \hat{\mathbf{L}}_g + \theta \mathcal{S}_0 = 0. \tag{27}$$

Table 1 Implementation algorithm in the AceGen

<p>1. Interpolate the field variables (components of displacement and concentration) using FEM shape functions</p> $d = \sum_I^N N_I d_I, \quad d_I := u_I, v_I, w_I, C_I, \quad d := u, v, w, C$ $d_e := \bigcup_I^N d_I = (u_1, v_1, w_1, C_1, \dots, u_N, v_N, w_N, C_N)$ <p>2. Initialize the Global Newton-Raphson using</p> $\mathbf{F}_{g(n+1)} = \mathbf{F}_{g(n)} = \alpha_n^3 \mathbf{I}$ $J_{g(n+1)} = \alpha_n^3$ $\hat{\mathbf{Q}}_{n+1} = \hat{\mathbf{Q}}_n$ $\mathbf{F}_{e(n+1)} = \mathbf{F}_{n+1} \cdot \mathbf{F}_{g(n)}^{-1}$ $\hat{\mathbf{C}}_{n+1} = \mathbf{F}_{e(n+1)}^T \cdot \mathbf{F}_{e(n+1)}$ <p>3. Compute</p> $\mathbf{S}_{n+1} = 2J_{g(n+1)} \mathbf{F}_{g(n+1)}^{-1} \frac{\partial \Psi_0}{\partial \hat{\mathbf{C}}_{n+1}} \mathbf{F}_{g(n+1)}^{-T} =$ $2J_{g(n+1)} \mathbf{F}_{g(n+1)}^{-1} \left(\frac{\partial \Psi^\infty}{\partial \hat{\mathbf{C}}_{n+1}} + \hat{\mathbf{Q}}_{n+1} \right) \mathbf{F}_{g(n+1)}^{-T}$ <p>4. Local (at Gauss point) equations: $\mathcal{R}_\alpha = \mathcal{R}_Q = 0$</p> <p>a. Solve the local problems (equations (32) and (5)) at Gauss points to find the internal variables α_{n+1} and $\hat{\mathbf{Q}}_{n+1}$</p> $\mathcal{R}_\alpha = \frac{\alpha_{n+1} - \alpha_n}{\Delta t} - Y \frac{K_1 C_{n+1}}{K_2 + C_{n+1}}$ $\mathcal{R}_Q = \hat{\mathbf{Q}}_{n+1} - \text{Exp}\left(\frac{-\Delta t}{\tau}\right) \hat{\mathbf{Q}}_n - \text{Exp}\left(\frac{-\Delta t}{2\tau}\right) \left(\frac{\partial \Psi^\infty}{\partial \hat{\mathbf{C}}_{n+1}} - \frac{\partial \Psi^\infty}{\partial \hat{\mathbf{C}}_n} \right)$ <p>b. Update $J_{g(n+1)}$, $\mathbf{F}_{g(n+1)}$, $\mathbf{F}_{e(n+1)}$ and $\hat{\mathbf{C}}_{n+1}$</p> <p>c. Compute $\mathbf{A} = \frac{\partial \alpha_{n+1}}{\partial C_{n+1}}$ and $\mathbf{B} = \frac{\partial \hat{\mathbf{Q}}_{n+1}}{\partial \mathbf{u}_{n+1}}$ which is later needed in tangent computation (step 6)</p> <p>5. Compute the total pseudo-potential by combining equations (7) and (8)</p> $\Pi = \int_{\mathcal{B}_0} \frac{1}{2} \mathbf{S}_{n+1} : \text{Grad} \delta \mathbf{C}_{n+1} + \int_{\mathcal{B}_0} D \text{Grad}(C_{n+1}) \cdot \text{Grad} \delta C_{n+1}$ <p>6. Compute the residuum vector of the element $\mathcal{R}_e = \frac{\partial \Pi}{\partial \mathbf{d}_e}$</p> <p>7. Compute the element stiffness matrix</p> $\mathcal{K}_e = \frac{\partial \mathcal{R}_e}{\partial \mathbf{d}_e} \Big _{\frac{\partial \alpha}{\partial \mathbf{d}_e} = \mathbf{A}, \frac{\partial \hat{\mathbf{Q}}}{\partial \mathbf{d}_e} = \mathbf{B}}$ <p>8. Global Newton-Raphson iteration: $(\mathcal{R}, \mathbf{d}, \mathcal{K}) = \bigcup^{\text{all elements}} (\mathcal{R}_e, \mathbf{d}_e, \mathcal{K}_e)$ DO WHILE $\ \mathcal{R}\ \geq \text{Tol}$ (Check the global convergence) Repeat steps (3) to (7) $\mathbf{d} \leftarrow \mathbf{d} + \Delta \mathbf{d}, \quad \Delta \mathbf{d} = -\mathcal{K}^{-1} \mathcal{R}$ END DO</p> <p>9. Go to the next time step and start from step (2)</p>
--

This leads to

$$\mathcal{S}_0 = \hat{\boldsymbol{\Sigma}} : \hat{\mathbf{L}}_g / \theta. \quad (28)$$

As discussed in Eq. (14), now one can understand why the presence of $\theta \mathcal{S}_0$ in Eq. (27) is necessary. Otherwise, a non-negative dissipation is not guaranteed. To clarify this issue more, the Eq. (27) is simplified by virtue of the fact that $\hat{\mathbf{L}}_g = \dot{\mathbf{F}}_g \mathbf{F}_g^{-1} = \frac{\dot{\alpha}}{\alpha} \mathbf{I}$, one can write

$$-3 \frac{\dot{\alpha}}{\alpha} \text{tr}(\hat{\boldsymbol{\Sigma}}) + \theta \mathcal{S}_0 = 0. \quad (29)$$

Referring to Eq. (4), it is obvious that $\frac{\dot{\alpha}}{\alpha} > 0$. Since the sign of $\text{tr}(\hat{\boldsymbol{\Sigma}})$ might varies, one can not judge at the beginning

if the first term in the left hand side of Eq. (29) is positive or negative. In fact the role of source term is to rule it out, if it is negative. This way, the condition of non-negative dissipation is fulfilled. A comparison between the growth driven by nutrient diffusion and the stress-regulated growth can shed more light on this point. In the former the growth function $\dot{\alpha}$ is exclusively ruled by concentration diffusion C according to Eq. (4), while in the latter $\dot{\alpha}$ is a function of stress. In the latter, there is the possibility to construct an always positive dissipation even in the absence of the source term ($\theta \mathcal{S}_0$) by taking, for example, $\dot{\alpha} = -\text{sign}(\text{tr}(\hat{\boldsymbol{\Sigma}})) f(\alpha, \hat{\boldsymbol{\Sigma}})$, in which $f(\alpha, \hat{\boldsymbol{\Sigma}})$ is generally a positive scalar-valued function of α and $\hat{\boldsymbol{\Sigma}}$. $\text{sign}(\square)$ is the Sign function whose value is either +1 or -1, see [16]. Such an evolution function can capture

Table 2 Model parameters and constants (Material property from [12,34])

Parameter	Symbol	Value	Unit
Biofilm initial height	H	60.0	micrometer
Biofilm initial			
Maximum width	W	300.0	micrometer
3D biofilm diameter	d	2.0	micrometer
Cylinders radius	R	2.5	mm
Cylinders distance	S	20.0	mm
Box length	L	30.0	mm
Biofilm density	ρ_b	60.0	kg/m ³
Reaction Constant			
In Monod law	K_1	10^{-5}	s ⁻¹
Reaction Constant			
In Monod law	K_2	4.0×10^{-5}	kg/m ³
Nutrient Concentration			
In Bulk fluid	C_f	4.0×10^{-3}	kg/m ³
Yield Constant			
In Monod law	Y	0.1	kg/kg
Diffusion coefficient	D	2×10^{-9}	m ² /s
Biofilm Young’s modulus	E	10	Pa
Biofilm Poisson ratio	ν	0.45	–
Biofilm relaxation parameter	τ	0.01	s

both growth and resorption processes driven by tensile and compressive stress, respectively.

Taking into account Eq. (27) in simplifying Eq. (26) one can realize that, the second law of thermodynamics holds true if the remained term $\hat{Q} : \dot{\hat{F}}$ in Eq. (26) is non-negative. With reference to [17], this can be satisfied by using a suitable evolution equation for the internal variable \hat{F} . A commonly used evolution equation for \hat{F} is

$$\dot{\hat{F}} = \mathbb{V} : \hat{Q}, \tag{30}$$

in which \mathbb{V} is a positive definite fourth order tensor relating to the viscous effect. It is obvious that such a condition on \mathbb{V} ensures that $\hat{Q} : \dot{\hat{F}} \geq 0$. Inspired by a one-dimensional Maxwell model with linear geometry, the internal variable \hat{Q} is modeled using a relaxation process whose characteristic relaxation time is τ , see [17]. Extension of a 1D linear spring-dashpot system to a 3D solid leads to an ordinary differential equation (ODE) as follows

$$\dot{\hat{Q}} + \frac{\hat{Q}}{\tau} = \frac{d}{dt} \left(\frac{\partial \Psi^\infty}{\partial \hat{C}} \right). \tag{31}$$

Following a procedure similar to what is described in [17], the solution of the ODE (31) using a mid-point

discretization scheme leads to a practical recursive formula

$$\hat{Q}_{n+1} = \exp\left(\frac{-\Delta t}{\tau}\right) \hat{Q}_n + \exp\left(\frac{-\Delta t}{2\tau}\right) \left(\frac{\partial \Psi^\infty}{\partial \hat{C}_{n+1}} - \frac{\partial \Psi^\infty}{\partial \hat{C}_n} \right). \tag{32}$$

It should be noted that the right hand side of Eq. (31) slightly differs from what has been taken in [17] in which the viscous response affects only the isochoric part of the deformation. Here, we assume that the entire deformation is subjected to the viscous effects without differentiating between the isochoric and volumetric parts of the deformation. The reason is that we are going to apply this growth model to biofilm growth which is an extremely slow process and it is expected to reach a zero stress-state in large time scales compared to the relaxation time. In such slow growth process, all residual stresses are released (dissipated). That is why biofilms can also be modeled as viscous fluid or potential flow, see [12], rather than a visco-elastic solid. It is obvious that in case of modeling the biofilm as a deformable solid, one can not capture the stress decay (relaxation) without incorporating the viscous effects. In the numerical example section, a continuous transition from a viscous fluid to an elastic solid will be observed by changing the relaxation time τ .

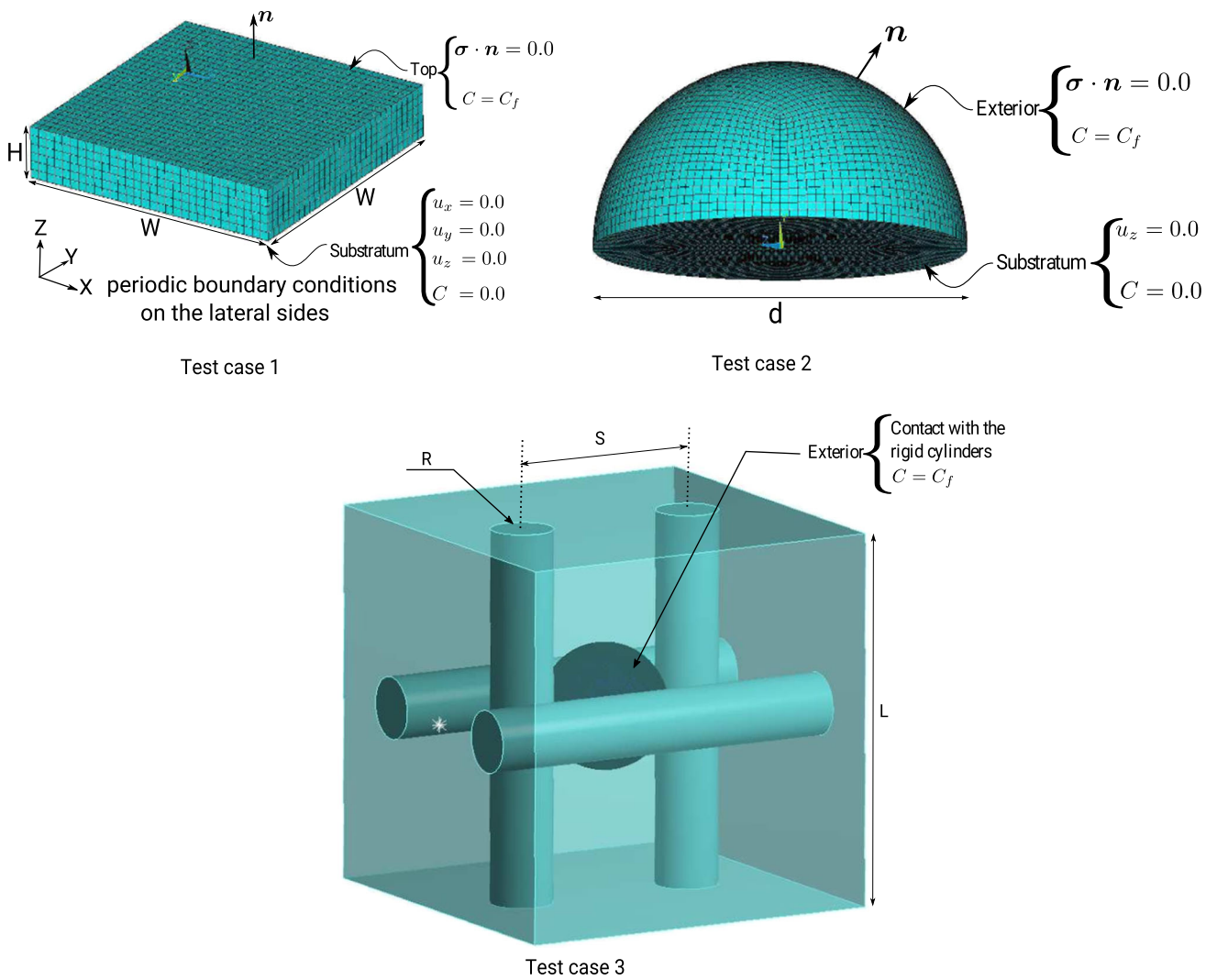
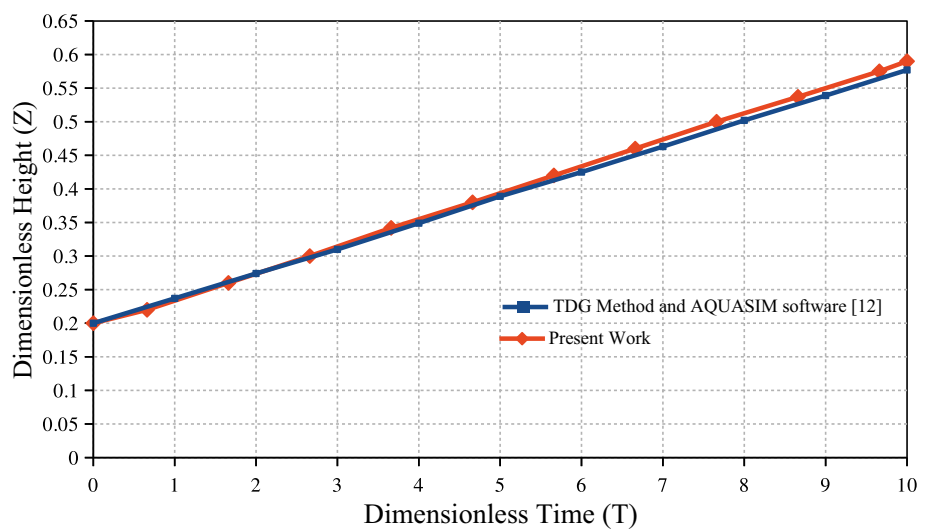


Fig. 2 Geometry of the test cases and the boundary conditions

Fig. 3 Validation of the height of the grown biofilm layer



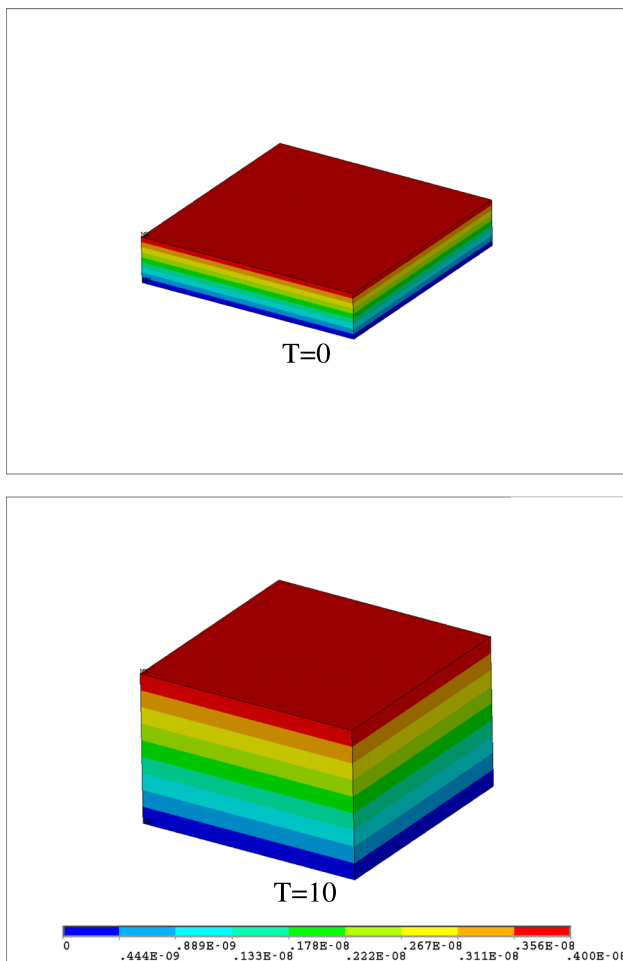


Fig. 4 Concentration field in the grown biofilm layer

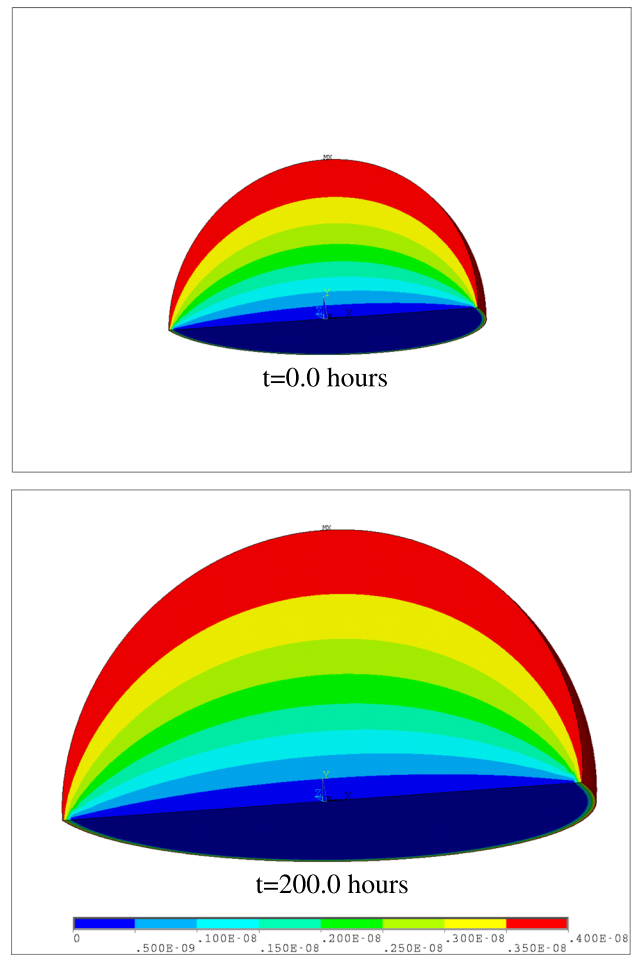


Fig. 5 Concentration distribution in biofilm

3 Numerical implementation using Ace-Gen

In this work, the formulation of a single element with multi-field (mechanical deformation, growth and nutrient concentration) has been implemented in Ace-Gen, see [19] which is a very powerful tool in automatic differentiation (hybrid symbolic/numeric differentiation). Its output is tailored to a FORTRAN subroutine which can be used as a user element in different FEM codes. We use Ansys since, one can benefit from its well-developed pre-processor, solver and post-processor.

The topology of the element is a common 3D brick element with 8 nodes. Each node has four degrees of freedom. Three of them represent the displacement vector \mathbf{u} components and the fourth one is allocated to the concentration field C which is scalar-valued. Furthermore, in the Gauss points there are two sets of internal variables: Tensor-valued variable \hat{Q} pertaining to the viscous behaviour as well as the scalar α which captures the biological growth. It is assumed that all internal and field variables are known at the previous time step. This is underlined using an n subscript for those

variables. An implicit Newton-Raphson is used as the solution procedure. The solution of the global system yields the current gradient deformation \mathbf{F}_{n+1} and concentration C_{n+1} . The objective is to find the update procedure for the current unknowns. To be concise, a summary of the entire algorithm is presented in Table 1.

4 Numerical examples

4.1 Test Case 1

In order to verify the validity of the developed model as well as the numerical implementation, the growth of a simple layer of biofilm is simulated and the results are compared with those reported in [12] using time-discontinuous Galerkin (TDG) method and the open source software AQUASIM which has been developed for 1D biofilms. The material constants and simulation parameters are chosen according to Table 2. The initial setup of the biofilm and the applied boundary conditions are depicted in Fig. 2.

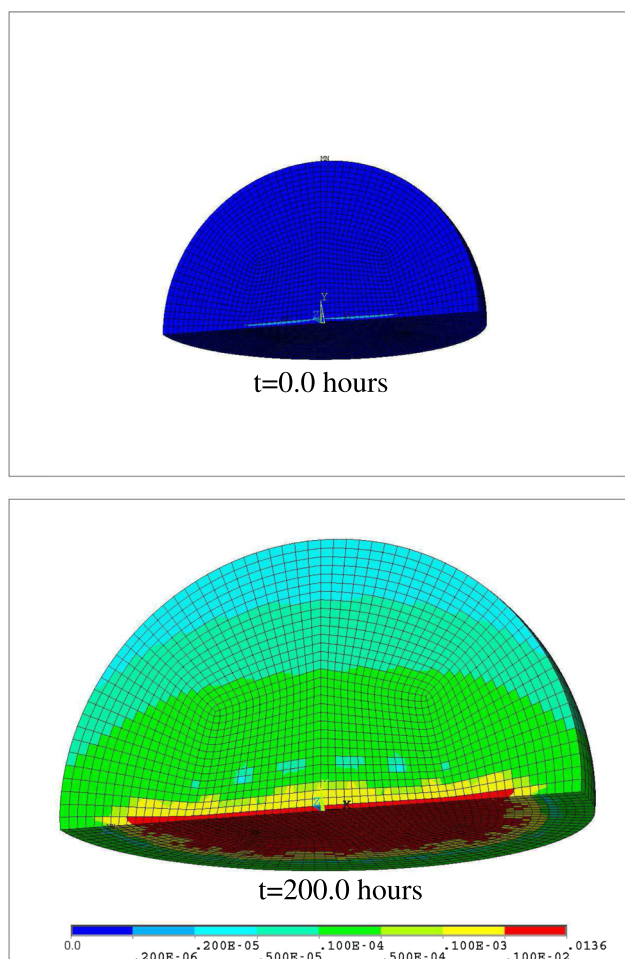


Fig. 6 Residual stress distribution in biofilm ($\tau = 0.01$)

In order to reproduce the plot in [12], the dimensionless time (horizontal axis) and height (vertical axis) are computed using $T = \frac{t}{t_{ref}}$ and $Z = \frac{Z}{Z_{ref}}$. It is taken $t_{ref} = 24$ hours and $Z_{ref} = W$. Figure 3 shows a good agreement between the results of the proposed method and those presented in [12].

Figure 4 displays the concentration field distribution in the biofilm. The linear variation of concentration across the Z-direction is even intuitively expectable, since the problem is in practice a 1D problem due to the applied boundary conditions. Looking to Fig. 4, one can see that while the biofilm movement is confined in X and Y direction, it can freely grow in the Z direction.

4.2 Test Case 2

In this example a truly 3D biofilm with an initial semi-spherical shape undergoing growth is modeled. The geometry of the model as well as the boundary condition are illustrated in Fig. 2. It is worth mentioning that in reality, most biofilms are submerged in a fluid from which they uptake the nutrient. It is commonly assumed that the transport mecha-

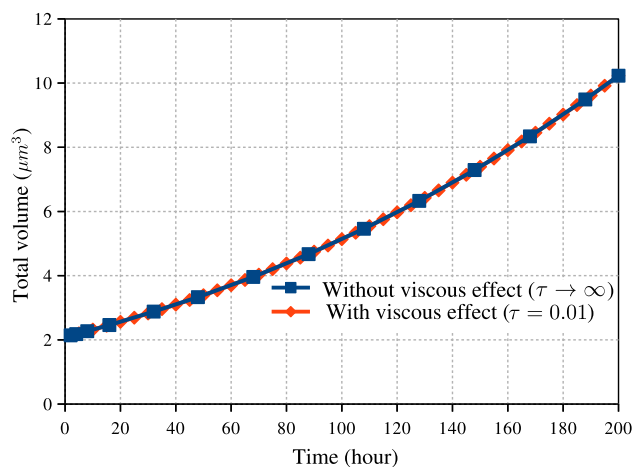


Fig. 7 Total volume of grown biofilm in time

nism in the fluid is convection-dominated [27]. Hence, it is well mixed and has a uniform concentration of the nutrient which is denoted by C_f . Here we have prescribed this bulk fluid concentration at the exterior of the biofilm geometry. This way, we exclude the fluid flow from the simulation and neglect boundary layer effects [22].

In Fig. 5 the contour of concentration field is shown in the beginning and the end of the time interval. For visualization purposes, one half of the biofilm is plotted. As expected, the concentration field maximum value lies at the outermost layer of the biofilm and it gradually tends to zero by approaching the substratum. It will result in a non-uniform growth, namely the outer layers of biofilm grow faster than the inner ones.

This non-uniform growth even manifest itself in the residual stresses pattern. Figure 9 demonstrates the dimensionless Von-Mises stress (σ/E) in the biofilm. One can notice that the boundary condition (constraint) along the substratum results in relatively large stress concentration there. The biofilm can not penetrate the substratum while it can freely spread parallel to it (Fig. 6).

The effect of different parameters on the biofilm growth is investigated. Since the growth happens in all three directions, the total volume of the biofilm is taken to be a quantitative indicator of the growth process rather than the displacement in a specific direction. Figure 7 shows the total volume of the grown biofilm during a time interval of 200 hours for different values of viscous parameter (relaxation time). The interesting point is that this parameter does not have an influence on the growth (displacement). The reason is that in our model, the growth is only derived and affected by the nutrient diffusion. Hence, neither stress field nor stress relaxation have an impact on the growth. Additionally, it is trivial that the steady state solution of a system is independent of the damping forces. However, the stress values depend on the viscous parameter, because this parameter determines “to what extent” and “how fast” the stresses are released (dissipated).

Fig. 8 Volume average of Von-Mises stress in biofilm

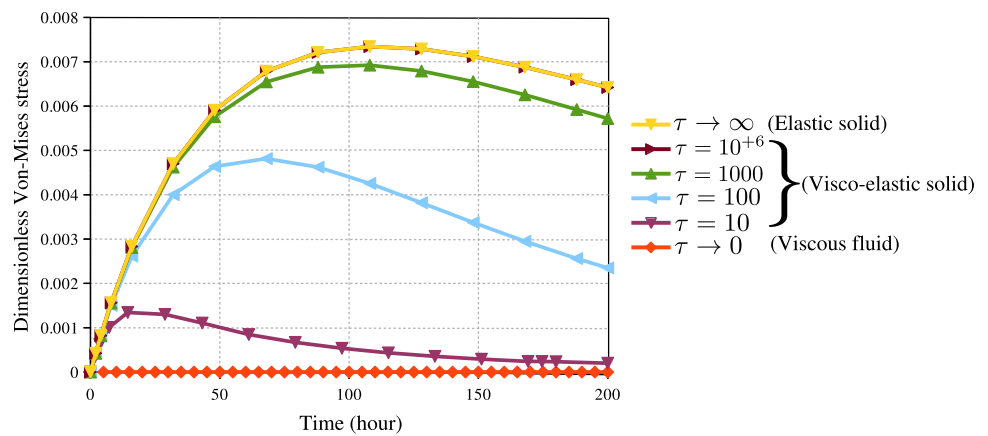


Figure 8 depicts the volume average of dimensionless Von-Mises stress (σ/E) in the entire biofilm. One can see the effect of the relaxation time on the residual stresses in the biofilm. The transition from a pure elastic solid (infinite relaxation time) to a viscous fluid (zero relaxation time) is interesting and intuitively expectable. As stated before, in biofilm growth phenomenon the stresses are nearly completely released due to the fact that the growth time scale is much larger than the characteristic relaxation time. The stresses should asymptotically approach zero values. The smaller the relaxation time, the faster the stresses decay.

4.3 Test Case 3

This test case is an interesting one inspired by an example presented in [2]. The idea is to investigate the growth of biofilms against rigid barriers. In such circumstances where the contact mechanics inherently plays a role in the model, the developed numerical implementation should be robust and stable enough in order to be capable of coping with the the strong nonlinearities arising from the contacts. Figure 2 shows a schematic view of the problem. It consists of an spheroid which starts to grow at the center of a cubic box. It has been surrounded by four rigid barriers. Such an arrangement of obstacles to the biofilm growth can mimic the real situation in water treatment systems [24] where a network of solid skeleton serves as the so-called biocarrier. The empty available space to be filled with the growing biofilm has a very complex geometry. A frictionless contact (for the sake of simplicity) is assumed between the biofilm surface and the rigid walls.

The biofilm undergoes a very severe shape change due to forces rising from the contact. Figure 9 shows dimensionless Von-Mises stress (σ/E) in the biofilm during growth process. For the visualization purposes, the cube and cylinders are transparent. The biofilm comes into contact with not only the cylinders but also the cube faces. One should note that quantitative comparison of the results here with those pre-

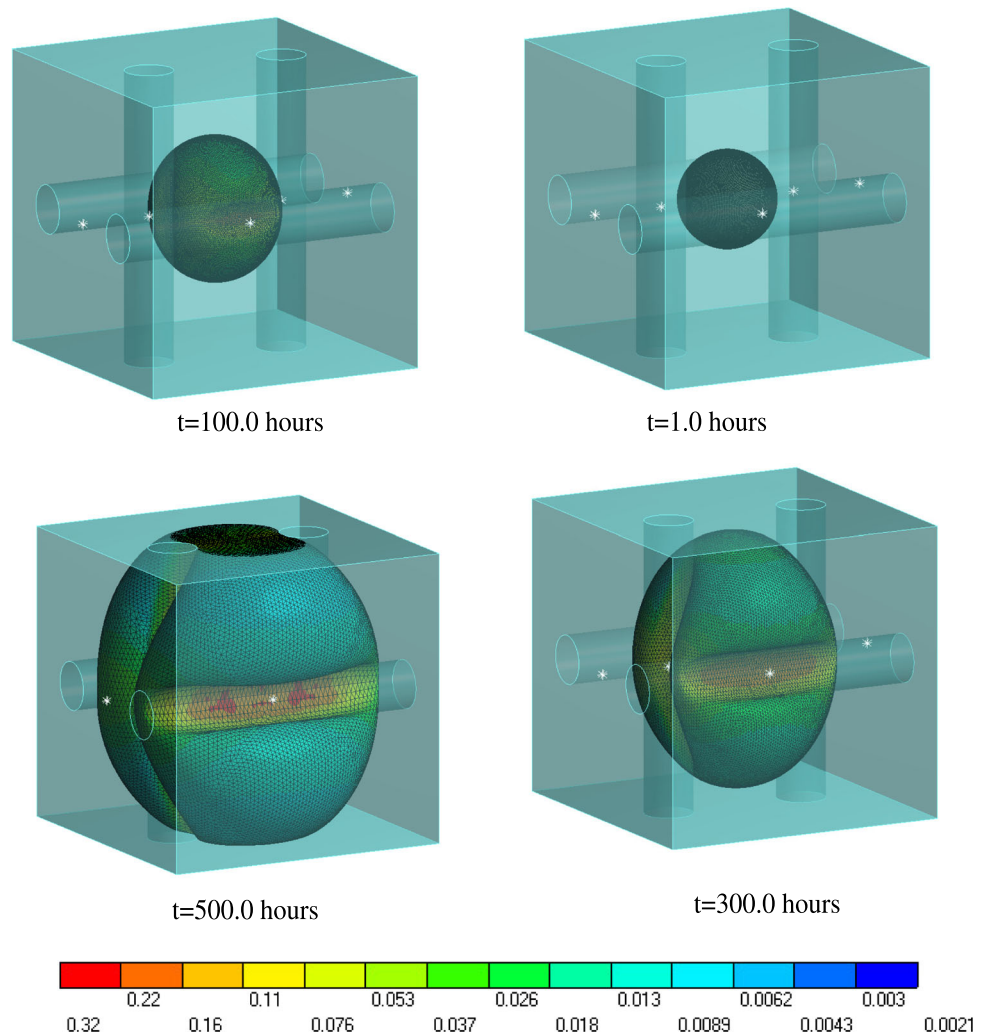
sented in [2] is not possible due to major differences between the two works. The reason is that in this work the growth is driven by the nutrient diffusion, whereas in [2] the diffusion equation is not present in the model. Moreover, the growth function in [2] is dependent on (basically restricted by) the hydrostatic pressure, while such a dependency does not exist in this work.

The interesting point is that unlike test cases 1 and 2 in which the biofilm grows freely without facing mechanical barriers, the mechanical stresses in the biofilm remain noticeable and do not decay that rapidly. This happens in spite of the the fact that all the material parameters are the same in three test cases and they are compared together based on an identical relaxation time ($\tau = 0.01$) associated with the viscous effects. In such cases, it is a good idea to incorporate the impact of the mechanical stresses on the growth function in addition to the nutrient diffusion. This can be a matter of further development of this work in future based on the well-developed framework of stress-regulated growth, see [36] and [8]. Such stress dependency renders the growth tensor F_g anisotropic. It means that there is a preferred direction for growth. Intuitively speaking, the biofilm is more likely to grow in the direction along which the compressive stress reaches its minimum value.

5 Conclusion

A mathematical model along with the numerical implementation in FEM framework was presented for the growth processes which are driven by the nutrient diffusion. The model was developed in a continuum-based framework and in the realm of finite visco-elastic growth. Special attention was paid to the concerns about the thermodynamical consistency of the model. An application of this model is the simulation of the biofilm growth. The numerical implementation was done using AceGen whose output was tailored as a user element for Ansys. Several numerical examples were

Fig. 9 Dimensionless Von-Mises stress in biofilm



carried out to show the robustness and performance of the proposed tool. This work can be extended in different directions. More complex growth function can be developed in order to account for the anisotropy rising from the presence of micro structure in the biofilm or the stress dependency. Furthermore, one can extend the model here to multi-species (heterogeneous) biofilm using mixture theories. Additionally, the impact of the surrounding fluid on the biofilm growth can be a matter of further development in the context of a fluid-solid interaction (FSI) problem.

References

1. Abi-Akl R, Abeyaratne R, Cohen T (2019) Kinetics of surface growth with coupled diffusion and the emergence of a universal growth path. *Proc R Soc A* 475:20180465
2. Albero BA, Ehret AE, Böhl M (2014) A new approach to the simulation of microbial biofilms by a theory of fluid-like pressure-restricted finite growth. *Comput Methods Appl Mech Eng* 272:271–289
3. Alpkvist E, Klapper I (2007) A multidimensional multispecies continuum model for heterogeneous biofilm development. *Bull Math Biol* 69:765–789
4. Bennett KC, Regueiro RA, Borja RI (2016) Finite strain elastoplasticity considering Eshelby stress for materials undergoing plastic volume change. *Int J Plast* 77:214–245
5. Chester SA, Anand L (2010) A coupled theory of fluid permeation and large deformations for elastomeric materials. *J Mech Phys Solids* 58:1879–1906
6. Coleman BD, Noll W (1963) The thermodynamics of elastic materials with heat conduction and viscosity. *Arch Ration Mech Anal* 13(1):167–178
7. Cowin SC, Hegedus DH (1976) Bone remodeling: theory of adaptive elasticity. *J Elast* 6(3):313–326
8. Cyron CJ, Humphrey JD (2017) Growth and remodeling of load-bearing biological soft tissues. *Meccanica* 52(3):645–664
9. Dillon R, Fauci L, Fogelson A, Gaver D (1996) Modeling biofilm processes using the immersed boundary method. *J Comput Phys* 129(1):57–73
10. Dortdivanlioglu B, Linder C (2019) Diffusion-driven swelling-induced instabilities of hydrogels. *J Mech Phys Solids* 125:38–52
11. Epstein M, Maugin GA (2000) Thermomechanics of volumetric growth in uniform bodies. *Int J Plast* 16(7):951–978
12. Feng D, Neuweiler I, Nackenhorst U (2017) A spatially stabilized TDG based finite element framework for modeling biofilm growth

- with a multi-dimensional multi-species continuum biofilm model. *Comput Mech* 59(6):1049–1070
13. Gebara F (1999) Activated sludge biofilm wastewater treatment system. *Water Res* 33(1):230–238
 14. Goriely A (2017) *The mathematics and mechanics of biological growth*. Springer, New York
 15. Harrigan TP, Hamilton JJ (1993) Finite element simulation of adaptive bone remodeling: a stability criterion and a time stepping method. *Int J Numer Method Eng* 36:837–854
 16. Himpel G, Kuhl E, Menzel A, Steinmann P (2005) Computational modeling of isotropic multiplicative growth. *Comput Model Eng Sci* 4(2):119–134
 17. Holzapfel GA (1999) On large strain viscoelasticity: continuum formulation and finite element applications to elastomeric structures. *Int J Numer Methods Eng* 39(22):3903–3926
 18. Klapper I (2002) Dockery J Finger formation in biofilm layers. *SIAM J Appl Math* 62(3):853–869
 19. Korelc J, Wriggers P (2016) *Automation of finite element methods*. Springer, Heidelberg
 20. Kreft JU, Booth G, Wimpenny JWT (1998) BacSim, a simulator for individual-based modeling of bacterial colony growth. *Microbiology* 144:3275–3287
 21. Kreft JU, Picioreanu C, Wimpenny JWT (2001) Individual-based modeling of biofilms. *Microbiology* 147:2897–2912
 22. Lardon LA, Merkey BV, Martins S, Dtsch A, Picioreanu C, Kreft JU, Smets BF (2011) iDynoMiCS: next-generation individual-based modeling of biofilms. *Environ Microbiol* 13(9):2416–2434
 23. Lear G, Lewis GD (2012) *Microbial biofilms: current research and applications*. Caister Academic Press, Norfolk
 24. Nicolella C, van Loosdrecht MCM, Heijnen JJ (2000) Wastewater treatment with particulate biofilm reactors. *J Biotechnol* 80(1):1–33
 25. Picioreanu C, van Loosdrecht MCM, Heijnen JJ (1998) A new combined differential-discrete cellular automaton approach for biofilm modeling: application for growth in gel beads. *Biotechnol Bioeng* 57(6):718–731
 26. Picioreanu C, Loosdrecht MCM, Heijnen JJ (1999) Discrete-differential modeling of biofilm structure. *Water Sci Technol* 39:115–122
 27. Picioreanu C, Loosdrecht MCM, Heijnen JJ (2000) Effect of diffusive and convective substrate transport on biofilm structure formation: a two-dimensional modeling study. *Biotechnol Bioeng* 69:504–515
 28. Rath H, Feng D, Neuweiler I, Stumpp NS, Nackenhorst U, Stiesch M (2017) Biofilm formation by the oral pioneer colonizer *Streptococcus gordonii*: an experimental and numerical study. *FEMS Microbiol Ecol*. <https://doi.org/10.1093/femsec/fix010>
 29. Reese S, Govindjee S (1998) A theory of finite viscoelasticity and numerical aspects. *Int J Solids Struct* 35(26):3455–3482
 30. Rittmann BE, McCarty PL (1980) Model of steady-state kinetics. *Biotechnol Bioeng* 22:2343–2357
 31. Rodriguez EK, Hoger A, McCulloch AD (1994) Stress-dependent finite growth in soft elastic tissues. *J Biomech* 27(4):455–467
 32. Sidoroff F (1974) un modle viscolastique non lineaire avec configuration intermediaire. *J de Mec* 13:679–713
 33. Simo JC (1987) On a fully three-dimensional finite-strain viscoelastic damage model: formulation and computational aspects. *Comput Methods Appl Mech Eng* 60(2):153–173
 34. Soleimani M, Wriggers P (2016) Numerical simulation and experimental validation of biofilm in a multi-physics framework using an SPH based method. *Comput Mech* 58(4):619–633
 35. Taber LA (1998) A model for aortic growth based on fluid shear and fiber stresses. *J Biomech Eng* 120(3):348–354
 36. Taber LA, Humphrey JD (2001) Stress-modulated growth, residual stress, and vascular heterogeneity. *J Biomech Eng* 123(6):528–35
 37. Trejo M, Douarche C, Bailleux V, Poulard C, Mariot S, Regard C, Raspaud E (2013) Elasticity and wrinkled morphology of *Bacillus subtilis* pellicles. *Proc Natl Acad Sci* 110:2011–2016
 38. Verner SN, Garikipati K (2018) A computational study of the mechanisms of growth-driven folding patterns on shells, with application to the developing brain. *Extreme Mech Lett* 18:58–69
 39. Wise SM, Lowengrub JS, Frieboes HB, Cristini V (2008) Three-dimensional multispecies nonlinear tumor growth: model and numerical method. *J Theor Biol* 253(3):524–543

Publisher's Note Springer Nature remains neutral with regard to jurisdictional claims in published maps and institutional affiliations.